

A New Theory for the Generation of the Equatorial Subsurface Countercurrents

MARKUS JOCHUM AND PAOLA MALANOTTE-RIZZOLI

Massachusetts Institute of Technology, Cambridge, Massachusetts

(Manuscript received 2 December 2002, in final form 14 October 2003)

ABSTRACT

An idealized numerical simulation of the tropical Atlantic Ocean is used to study the dynamics of an Atlantic subsurface countercurrent, the South Equatorial Undercurrent (SEUC). The particular structure of the SEUC between 28° and 10°W allows for a reformulation of the transformed Eulerian mean (TEM) equations with which the momentum balance of the SEUC can be explored. With this modified TEM framework, it is shown that between 28° and 10°W the SEUC is maintained against dissipation by the convergence of the Eliassen–Palm flux. The source of this Eliassen–Palm flux is the tropical instability waves that are generated along the shear between the Equatorial Undercurrent and the South Equatorial Current.

1. Introduction

The Atlantic and Pacific Oceans both feature two narrow subsurface countercurrents that flow eastward several degrees poleward of either side of the equator. As they cross the basin, their core rises across isopycnals and shifts poleward. Stroup (1954) already noted the sloping isopycnals below the Pacific thermocline that are associated with these countercurrents, and Tsuchiya (1975) described them as steady features that are distinct from the surface intensified Northern or Southern Equatorial Countercurrents. Later they were described in the Atlantic by Cochrane et al. (1979). Even though their structure is very similar in both oceans, these jets were given different names. In the Pacific they are called subsurface countercurrents (SCCs) or Tsuchiya jets, whereas in the Atlantic they are commonly referred to as the Northern and Southern Equatorial Undercurrent (NEUC and SEUC). This different labeling often leads to confusion and especially the choice for the Atlantic is unfortunate since it suggests a dynamic similarity to the Equatorial Undercurrent. However, we will use this terminology for the remainder of this paper.

In the Pacific, Rowe et al. (2000) recently provided a review of the available observations related to the SCCs and analyzed an extensive set of hydrographic and Acoustic Doppler Current Profiler (ADCP) data. They found that the SSCs carry about 14 Sv (1 Sv $\equiv 10^6 \text{ m}^3 \text{ s}^{-1}$) of water across the basin and that their core densities decrease as they shoal from 300-m depth in the west to 150-m depth in the east. The main cores

with maximum speeds of 0.4 m s^{-1} are located at approximately 4°S and 4°N in the western basin and they migrate poleward as they move east. Fewer observations are available in the Atlantic. At 30°W, Cochrane et al. (1979) find for the SEUC a transport of 15 Sv (based on three hydrographic sections in February and one section in August). On the other hand, Schott et al. (1998) determine the transport at 35°W to be 2 Sv (based on four ADCP sections, two in October, one in March, and one in June). These values are hard to reconcile and are probably due to the aliasing of the tropical wave field. Furthermore, Cochrane et al. (1979) face the problem of choosing a level of no motion, and the Schott et al. (1998) measurements of the SEUC are so close to the western boundary that one cannot exclude the possibility that energy from the North Brazil Current (NBC) influences the observations. A recently published dataset by Bourles et al. (2002) suggests that during summer the SEUC has a transport of approximately 4 Sv at 35°, 23°, and 10°W. As in the Pacific, transport estimations for the NEUC are very difficult since the NEUC and the North Equatorial Countercurrent (NECC) are difficult to separate (Fig. 1). The Bourles et al. (2002) observations show that the core of the SEUC is approximately at 4°S and has a maximum speed of 30 cm s^{-1} (during summer). Like its counterpart in the Pacific, the SEUC shoals on its way from west to east cross isopycnals, but the data are inconclusive on the poleward migration of the SEUC. Two different sections at 10°W show the SEUC core once at 4°S, once at 5.5°S. Since the Atlantic basin is much smaller than the Pacific basin, it is conceivable that the poleward migration of the SEUC is not even observable.

Similar to the observations, much more numerical and theoretical work has been done on the Pacific SCCs than

Corresponding author address: Markus Jochum, MIT, Room 54-1410, 77 Massachusetts Avenue, Cambridge, MA 02139.
E-mail: markus@ocean.mit.edu

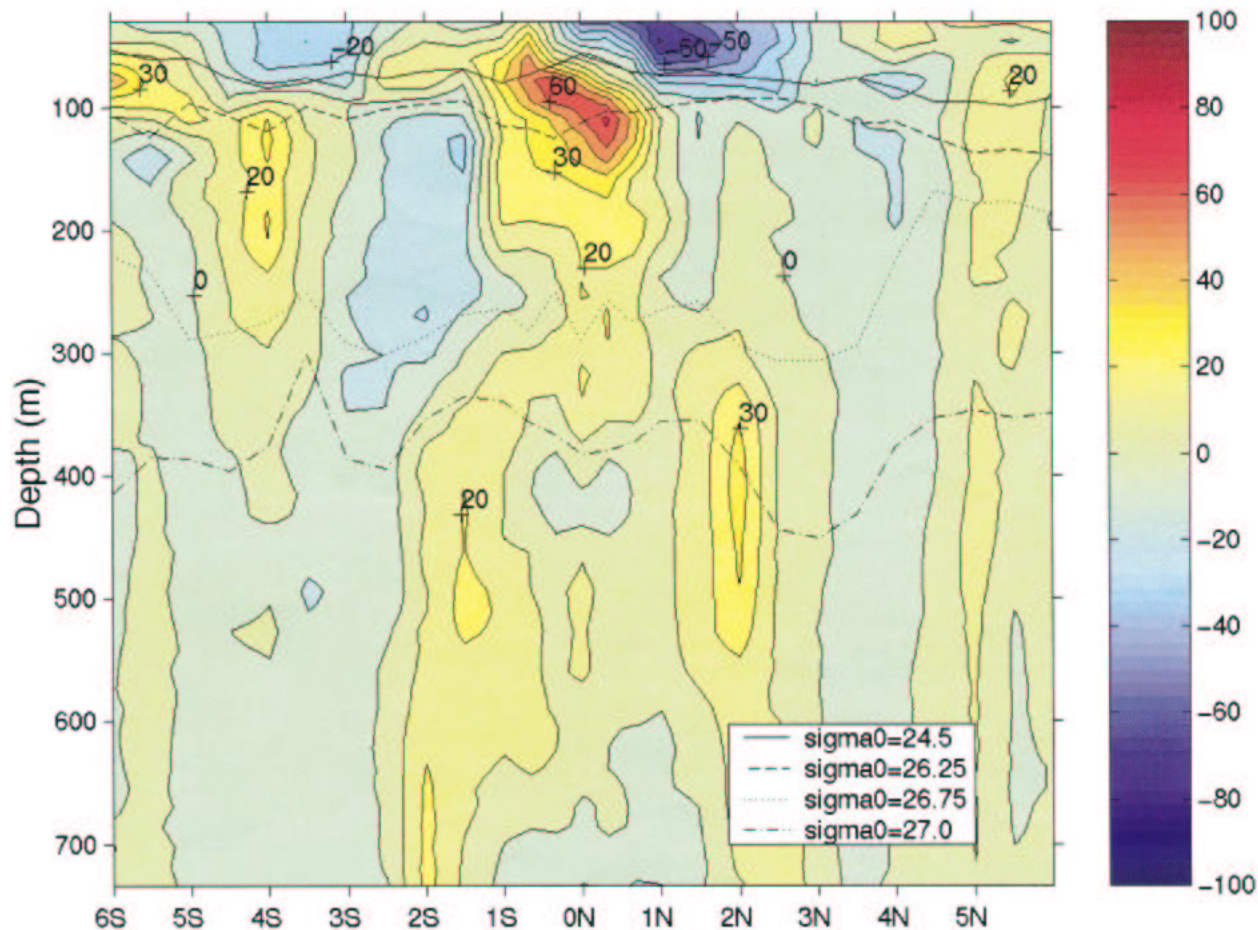


FIG. 1. The zonal velocity across 23°W (Bourles et al. 2002; contour lines every 10 cm s^{-1}). Yellow–red denotes eastward flow and green–blue denotes westward flow. The thick black lines indicate the depth of the isopycnals. Note the SEUC at 4°S and the NEUC at 5°N.

on the Atlantic SEUC and NEUC. The work of Donohue et al. (2002) showed that an eddy-resolving numerical model of the Pacific ocean can reproduce the cross-isopycnal shoaling of the SSCs but not the poleward migration of the cores. A detailed comparison for the respective jets in Atlantic has yet to be made, but currently the available database is not sufficient.

Even though the SSCs are reasonably well sampled and reproduced in numerical models, their dynamics is still not completely understood. Because their core is below the thermocline, it is commonly assumed that they cannot be directly wind-driven. McPhaden's (1984) analytical approach, which is based on McCreary's (1981) linear wave model, explains the SSCs as a balance between vertical diffusion of relative vorticity and advection of planetary vorticity. The limitation of this diffusive solution is that the SSC cores are not separate velocity maxima, but weak sidelobes of eastward velocities extending from the Equatorial Undercurrent (EUC).

Johnson and Moore (1997) use a 1 and 1/2-layer model to explain the spatial structure of the SSCs as inertial

jets. Because the flow conserves potential vorticity, the eastward shoaling of the equatorial thermocline is compensated by the poleward migration of the jets. While this theory explains the observed poleward migration of the core, it cannot account for the diapycnal processes that force the SSCs to rise across isopycnals. Furthermore, it requires a remote forcing mechanism, the nature of which is not addressed in their manuscript.

Like McPhaden (1984), Marin et al. (2000) explain the SSCs as a locally forced phenomenon. They develop a two-dimensional model of the equatorial thermocline with a prescribed density structure to study the dynamics of the SSCs. It is found that, after adding a localized diapycnal forcing, a secondary circulation develops and the SSCs can be explained as the result of conservation of angular momentum. This theory can account for the observed shoaling of the SSCs across isopycnals and indicates that local ageostrophic processes may be important for the SSCs. The physics of the localized diapycnal forcing, however, has yet to be discussed. In two follow-up papers, the authors (Hua et al. 2003; Marin et al. 2003) further develop the connection between

the SSCs and the conservation of angular momentum in a fully three-dimensional model, demonstrating that their theory is not simply an artifact of the two-dimensional model. They show that the strength of the SSCs depends on the properties of the water that is subducted in the subtropics and then feeds the equatorial thermocline. However, the physical process that provides the diapycnal forcing is left unexplained.

Based on the results of a hierarchy of idealized numerical models, McCreary et al. (2002) explains the SSCs as being remotely forced by the Indonesian throughflow and upwelling along the eastern boundaries and in the interior. As such, the SSCs are an integral part of the interhemispheric circulation and local processes as required by McPhaden (1984) and Marin et al. (2000) are not important. This study furthermore suggests that the SSCs are geostrophic currents along arrested fronts. Such fronts are generated when Rossby wave characteristics, carrying the information of the eastern boundary, intersect in the interior ocean. Like the Johnson and Moore theory (1997) this theory focuses on remote forcing and is able to explain the poleward migration of the SSCs. McCreary et al. (2003), however, provides a forcing mechanism for the SSCs: the upwelling along the eastern boundaries. In analogy with the Indonesian Throughflow in the Pacific, the SSCs's counterparts in the Atlantic (SEUC and NEUC) could be driven by the meridional overturning circulation (McCreary et al. 2003). The appeal of the McCreary et al. (2003) theory lies in its analytical framework that predicts the structure of the SCCs, which is confirmed by the results of their layer models. Studies with primitive equation models, however, did not show any effect of the Indonesian Throughflow on the SCCs (T. Tozuka 2001, personal communication) or the meridional overturning circulation on the SEUC and NEUC (Jochum 2002). This suggests that local forcing as suggested in McPhaden (1984) and Marin et al. (2000) may be at least as important as remote forcing.

All of the theories described above explain aspects of the SCCs, but none of them is able to fully explain the jets. The present study gives further support to the idea that local forcing is important for the dynamics of at least the SEUC. It does not claim to provide a complete theory for the SEUC, but it explains the shoaling of the SEUC cores across isopycnals and gives evidence that the SEUC is at least in some parts the result of a balance between dissipation and diapycnal eddy fluxes. These eddy fluxes could be the physical process that provide the diapycnal mixing required in Marin et al. (2000). The potential importance of eddy fluxes has already been noted by Johnson and Moore (1997), Rowe et al. (2000), McCreary et al. (2003), and N. Sugihara (2001, personal communication) but has yet to be explored in detail.

After the numerical model that is used in this study is explained in the next section, three pieces of evidence are provided that suggest that tropical instability waves

(TIWs), at least partly, drive the SEUC. On their own, none of these three pieces are conclusive; but together they strongly suggest a connection between TIWs and the SEUC. Section 3 demonstrates that suppressing the advection of momentum in the model removes simultaneously the TIWs and the SEUC. Section 4 shows that in the core of the SEUC dissipation is balanced by the Eliassen–Palm flux of the TIWs, and section 5 describes how the spatial structure of the TIWs is reflected in the location of the SEUC core. The last section provides a summary of the results.

2. The model configuration

The following model setup allows for the generation of the SEUC, but it was initially designed to study the generation of North Brazil Current rings (Jochum and Malanotte-Rizzoli 2003). This explains some of the particular choices that were made for the resolution and the boundary conditions.

The model is based on the Modular Ocean Model 2b (MOM2b) code. The domain is an idealized basin from 25°S to 30°N in latitude and from 70°W to 15°E in longitude, with a flat bottom at 3000 m. The resolution is $\frac{1}{4}^\circ$ by $\frac{1}{4}^\circ$ at the western boundary between the equator and 12°N, and becomes coarser toward the eastern, northern, and southern boundaries: the latitudinal resolution is reduced from $\frac{1}{4}^\circ$ to 1° at the meridional boundaries, and the longitudinal resolution is reduced from $\frac{1}{4}^\circ$ to 1.5° at the zonal boundaries (see Fig. 2 for an illustration of the resolution). There are 30 levels in the vertical direction, with a 10-m resolution in the top 100 m. The resolution along the path of the SEUC is approximately $\frac{1}{2}^\circ$ in latitude, $\frac{3}{4}^\circ$ in longitude, and 20 m in the vertical direction. Studies with $\frac{1}{3}^\circ$ and even $\frac{1}{12}^\circ$ resolution showed no increase in SEUC transport (Kroeger 2001).

Horizontal mixing is done by a Laplacian scheme with the eddy viscosity and diffusivity being linearly dependent on the resolution: from $200 \text{ m}^2 \text{ s}^{-1}$ for $\frac{1}{4}^\circ$ to $2000 \text{ m}^2 \text{ s}^{-1}$ for 1° resolution. In the vertical direction, a Richardson number–dependent vertical mixing scheme is used. Unstable temperature gradients are eliminated by mixing heat vertically to a depth that ensures a stable density gradient.

The initial condition is a state of rest. Salinity remains constant in time and space at a value of 35 psu. This choice simplifies the analysis and does not significantly distort the upper-layer circulation because in the tropical Atlantic, the observed temperature induced density gradients are much larger than the salinity induced density gradients (Philander 1990). The wind stress (Hellerman and Rosenstein 1983) is shown in Fig. 2. The initial temperature distribution is symmetric about the equator and is essentially a zonally averaged, idealized climatology (as shown in Fig. 1 of Liu and Philander 1995). This profile is also used at the surface to restore the surface temperature with a 40-day relaxation time. The

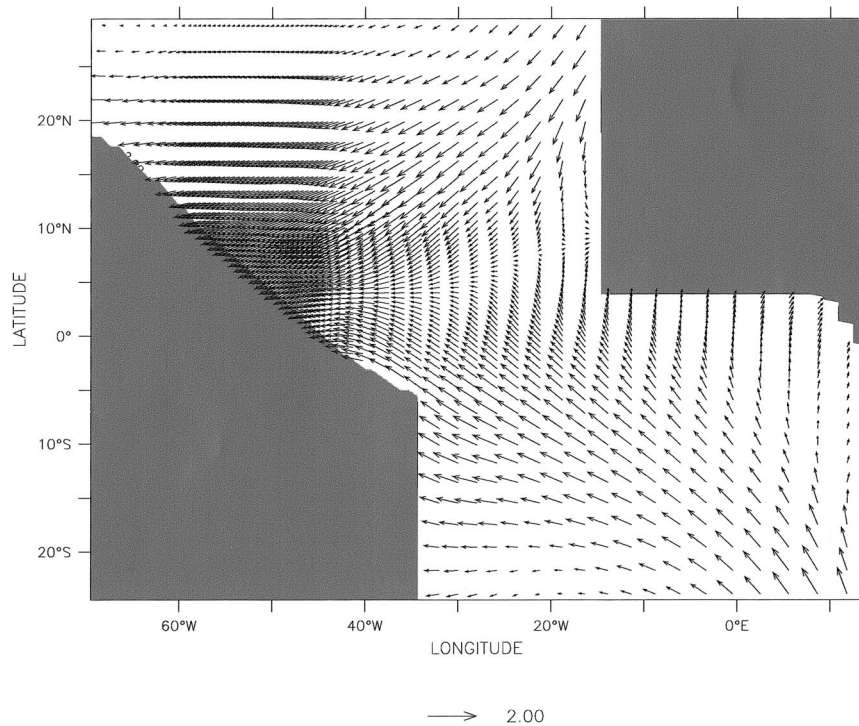


FIG. 2. The yearly mean wind stress over the domain. Note the high resolution along the Brazilian coast and the equator (for the sake of clarity only every fourth grid point is shown). The Caribbean Sea is not part of the model domain.

experiment was integrated for 18 yr before any analysis was performed (because of the fast tropical adjustment and the initial stratification this a sufficient spinup time; see Liu and Philander 1995).

The effect of the global Meridional Overturning Circulation (MOC) was represented by open boundary conditions (OBC). The working assumption is that the upper-layer circulation in the tropical Atlantic Ocean is the superposition of the purely wind-driven circulation and the return flow of the MOC (see Jochum and Malanotte-Rizzoli 2001 for a detailed discussion). It is known that OBC render ill posed the problem of solving the primitive equations (Oliger and Sundstrom 1978). Nevertheless one can make progress if the errors that are introduced by the OBC are small enough and do not grow in time [see Spall and Robinson (1989) for a detailed discussion]. At the open boundaries, the temperature and the barotropic streamfunction are specified. Using geostrophy, the model then calculates the velocity field (Stevens 1990). The barotropic streamfunction and temperature at the open boundaries are taken from the steady-state solution of an experiment with closed boundaries and without a deep thermohaline circulation. To make sure that the effects of the artificial boundaries do not overly affect the interior solution, the basin for this experiment extended from 40°S to 40°N.

To simulate the throughflow of the MOC return flow, the barotropic streamfunction is set to 0 at the western boundary and to 15 Sv at the eastern boundary, so that

15 Sv flow into the South Atlantic all along the southern boundary and leave the North Atlantic in the northwest corner through a western boundary current (see Fig. 3). These 15 Sv enter the domain across the southern boundary in the upper 1000 m of the water column; their exact spatial distribution depends on the specification of the temperature field at the southern boundary. The total inflow is roughly consistent with numbers from the literature (Schmitz and McCartney 1993). We did not attempt to simulate a deep western boundary current because we wanted to focus on the upper-layer circulation. The experiment as it is described above will be referred to as Exp1. To isolate particular processes, two more experiments have been performed. They are identical to Exp1 except that the advection of momentum is removed (Exp2) or it is driven with steady winds (Exp3).

3. The structure of the SEUC in the model

Figure 4 reveals the eastward EUC at 1°S, flanked by the two westward branches of the South Equatorial Current (SEC). The deep lobes of the SEC and the off-equatorial position of the EUC are explained by the downward and southward advection of momentum (Philander 1990). At 5°S the SEUC can easily be identified as the isolated core of eastward velocity at 200-m depth. The core is here defined as local maximum of the zonal velocity in the y - z plane. The NEUC, like the Northern

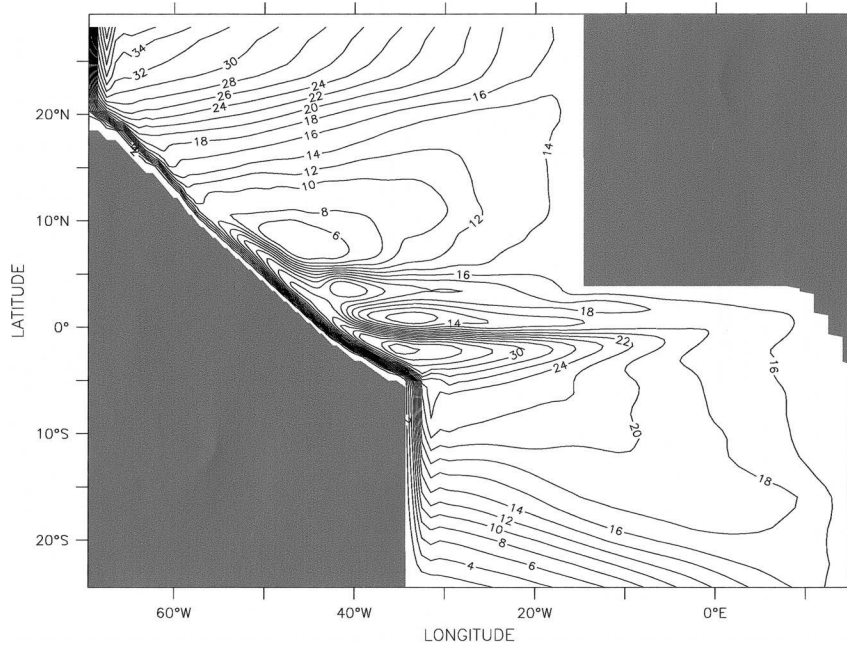


FIG. 3. The time-mean barotropic streamfunction (S_v). The streamlines entering the basin along the southern boundary and leaving it at the northwest corner represent the warm water return flow of the MOC.

Subsurface Countercurrent (NSCC) in the Pacific, cannot be distinguished from the lower part of the NECC (at 4°N); therefore this work focuses on the SEUC. Since the SEUC rises across isotherms there is not a single best surface to display the horizontal structure of the

SEUC. Here, the flow on the 17°C isotherm is chosen because it displays the three distinct regions of the SEUC (Fig. 5): the flow west of 28°W is under the influence of western boundary recirculations, between 28° and 5°W the flow is parallel to the equator and

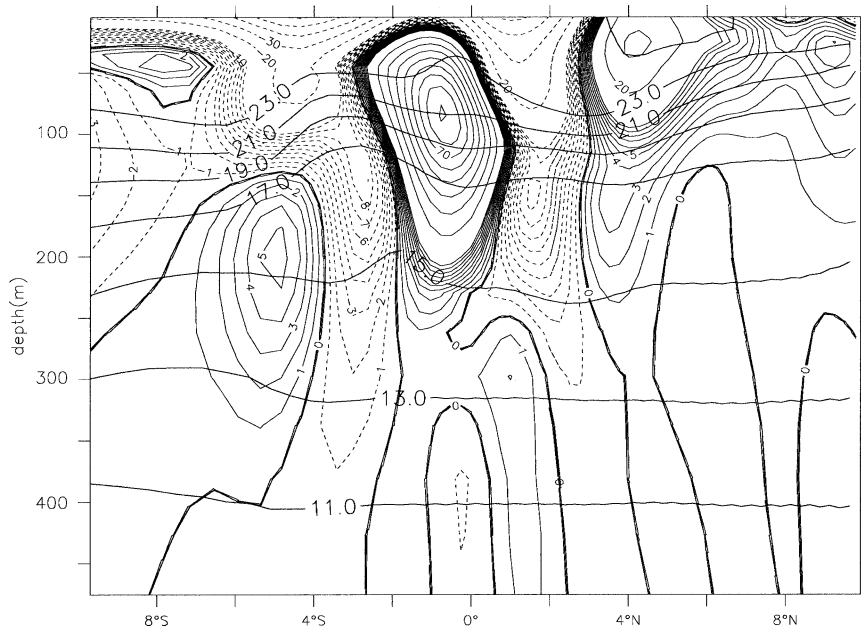


FIG. 4. The zonal mean velocity at 25°W . The SEUC can be seen at 5°S . The NEUC, which can be seen at 5°N , merges with the lower part of the NECC. The contour interval between -10 and 10 cm s^{-1} is 1 cm s^{-1} ; it is 10 cm s^{-1} everywhere else. The overlaying thick lines are isotherms with a contour interval of 2 K .

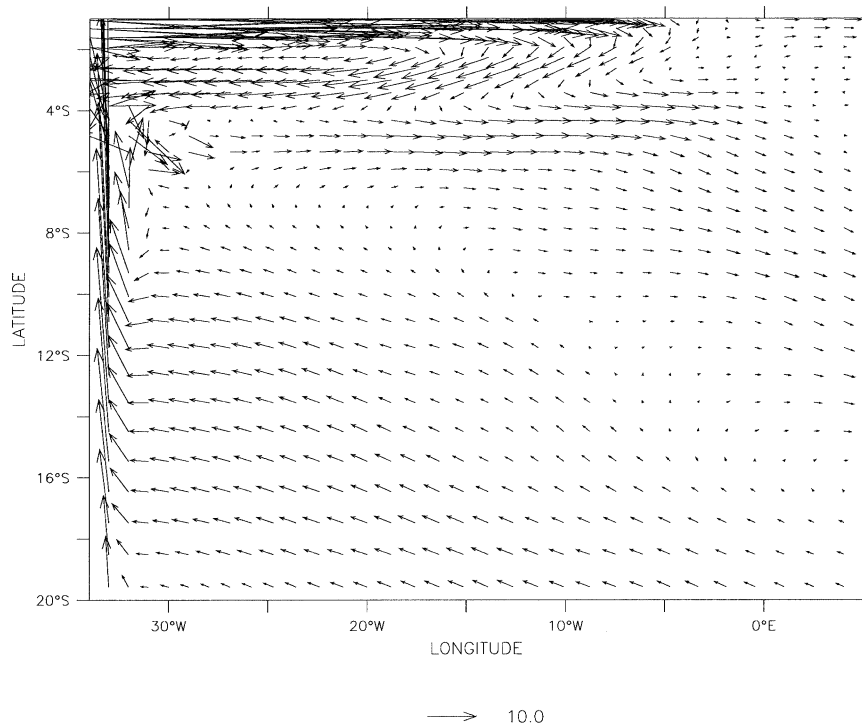


FIG. 5. The mean velocity (cm s^{-1}) on the 17°C isotherm between 20° and 1°S .

thereafter it turns southeast. Between the EUC at 1°S and the SEUC is the westward SEC, and it appears that the EUC provides at least some water for the SEUC in the interior. This becomes clearer by studying the potential vorticity (PV) distribution [defined as $-(f +$

$\zeta)T_z$; Fig. 6], which shows a broad band of low-PV water between the equator and the core of the SEUC, similar to the observations in the Pacific (Rowe et al. 2000).

The model barotropic streamfunction (Fig. 3) suggests that the southeastward extension of the SEUC is

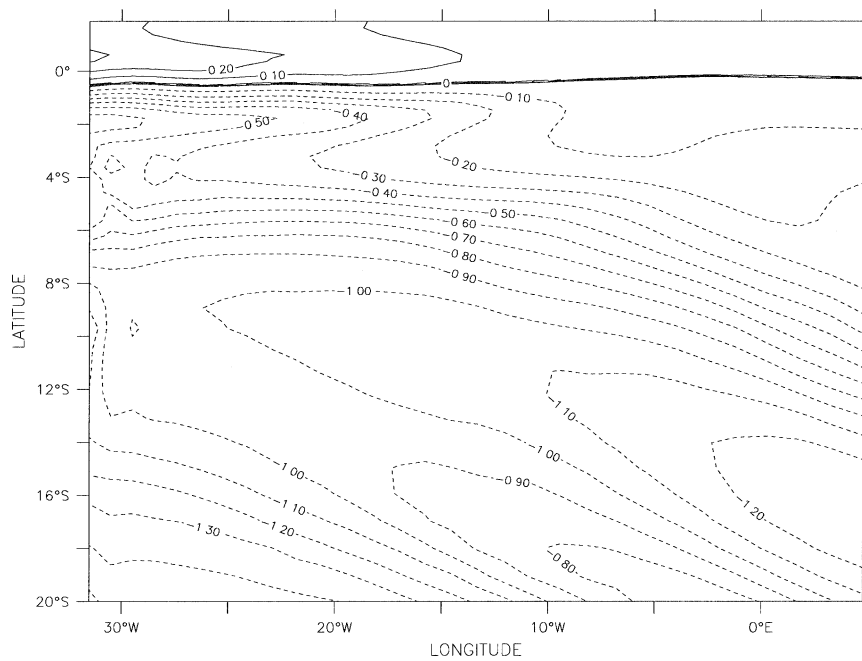


FIG. 6. The potential vorticity on the 17°C isotherm between 20°S and 2°N .

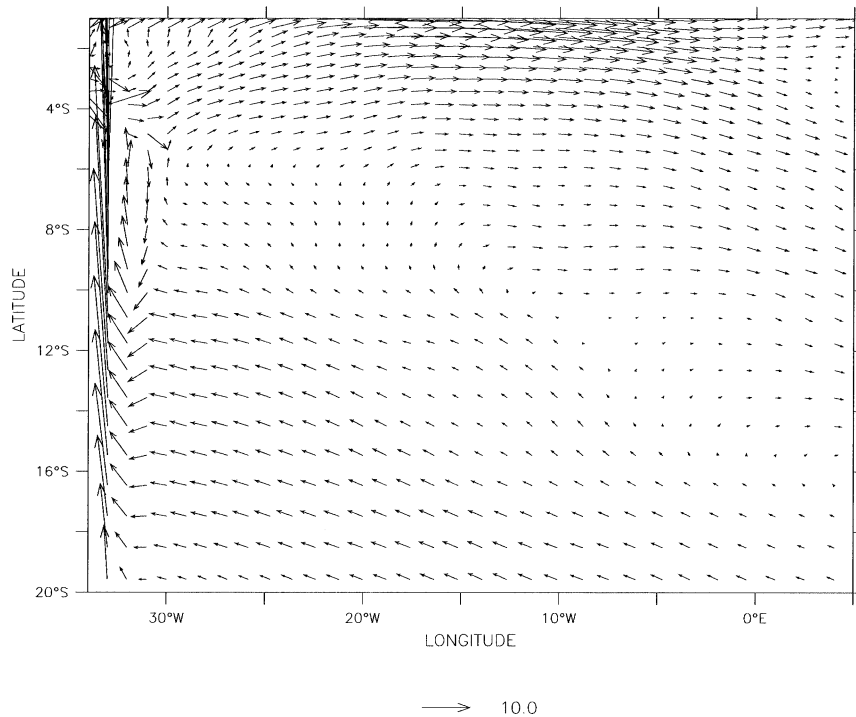


FIG. 7. The mean velocity on the 17°C isotherm between 20° and 1°S for the experiment without advection of momentum.

part of the equatorial gyre and is directly forced by the wind as already suggested by Mayer et al. (1998) in a study based on XBT data. To verify this, Exp1 was repeated, omitting the nonlinear terms in the momentum equation. In both experiments, the interior flow south of 6°S is identical (cf. Figs. 5 and 7). The main difference is that in the linear experiment the southeastward branch of the equatorial gyre is fed by the SEUC, whereas in the linear run it is fed by a broad EUC. Philander (1990) has already shown that the EUC in a linear solution is much broader than in a nonlinear solution because the poleward diffusion of momentum is no longer countered by equatorward advection of momentum in the thermocline. The comparison between the two experiments suggests that east of the western boundary regime, the SEUC is under two different dynamical regimes, only the western part requiring advection of momentum; in the east, the SEUC surfaces and feeds the directly wind-driven gyre. This eastward broadening of the SEUC is strikingly similar to the broadening of the SSCs in the study of McCreary et al. (2003), which suggests that at least in the eastern domain the structure of the SEUC is determined by the arrested Rossby wave fronts (McCreary et al. 2003). In the interior of the domain, however, the nonlinearities in the momentum equations lead to a sharpening of the SEUC, which requires further explanation. Even though the SEUC in the model is in geostrophic balance with a Rossby number of approximately 0.05, it vanishes as a separate jet upon suppression of advection of momentum. This sug-

gests that the meridional density gradient which drives the SEUC is determined by a nonlinear process. It is argued here that the TIWs are exactly this process. Like the separate SEUC core, they are absent in the linear experiment. Furthermore, they are most energetic near the equator and they are known to transport heat meridionally (Hansen and Paul 1984). The remainder of this manuscript will be devoted to the study of the narrow SEUC core in the interior of the basin and its connection to the TIWs.

A section of temperature and velocity along the core of the SEUC is shown in Fig. 8. Overlying the SEUC is the core of the SEC and adjacent on the SEUC's western end is the NBC. It can be seen that, as in the observations, the core water of the SEUC becomes warmer as the SEUC penetrates east. However, as one would expect from a geostrophically balanced flow, the velocity vectors in Fig. 8 point along isotherms and not along isotachs. Thus, the water moves adiabatically as it enters the SEUC above the core, crosses the core and leaves it below the core.

The surfacing of the SEUC at 5°W is consistent with the observations by Bourles et al. (2002), which do not show a subsurface core of the SEUC at 0°W. At each longitude between 28° and 5°W, the SEUC in the model has a mean transport of approximately 2 Sv and a maximum zonal velocity of 12 cm s⁻¹, which is clearly lower than the observed values (4 Sv and 30 cm s⁻¹; Bourles et al. 2002). From these observations we estimate the Rossby number to be between 0.2 and 0.4.

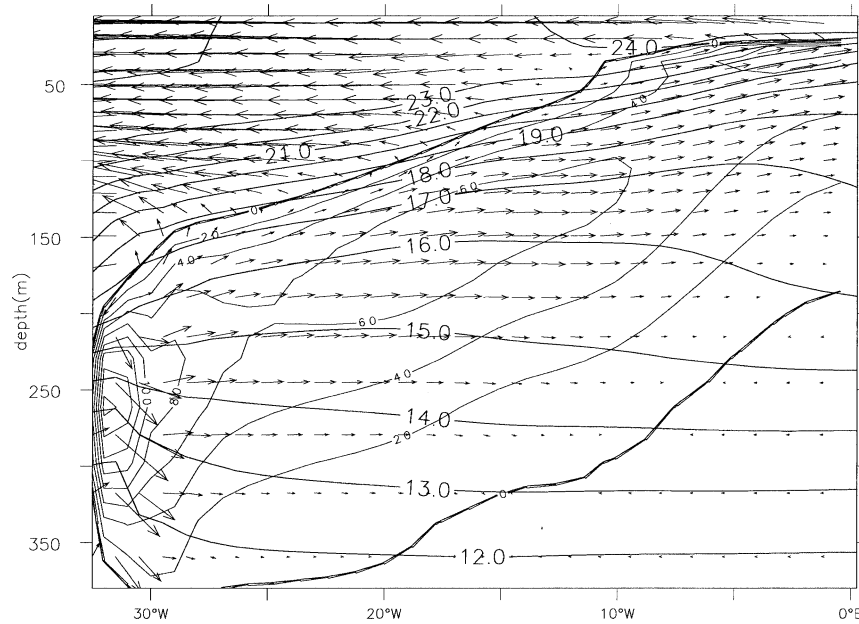


FIG. 8. The time-mean velocity along the core of the SEUC at 5°S. The contour lines show the magnitude of the flow in the SEUC (cm s^{-1}), and the arrows indicate the direction. The overlying thick lines show the mean temperature, from 12°C at 350-m depth to 24°C at the surface.

Figures 5–8, which all show aspects of the time-mean circulation, and the analysis of observations by Rowe et al. (2000) suggest that eddy fluxes are relevant to the maintenance of the SEUC. Further indication for the

importance of eddies for the SEUC can be found in Fig. 9. The figure shows that the narrow part of the SEUC is positioned at the poleward edge of a wave train. Interestingly, the broad southeastward flow and the narrow

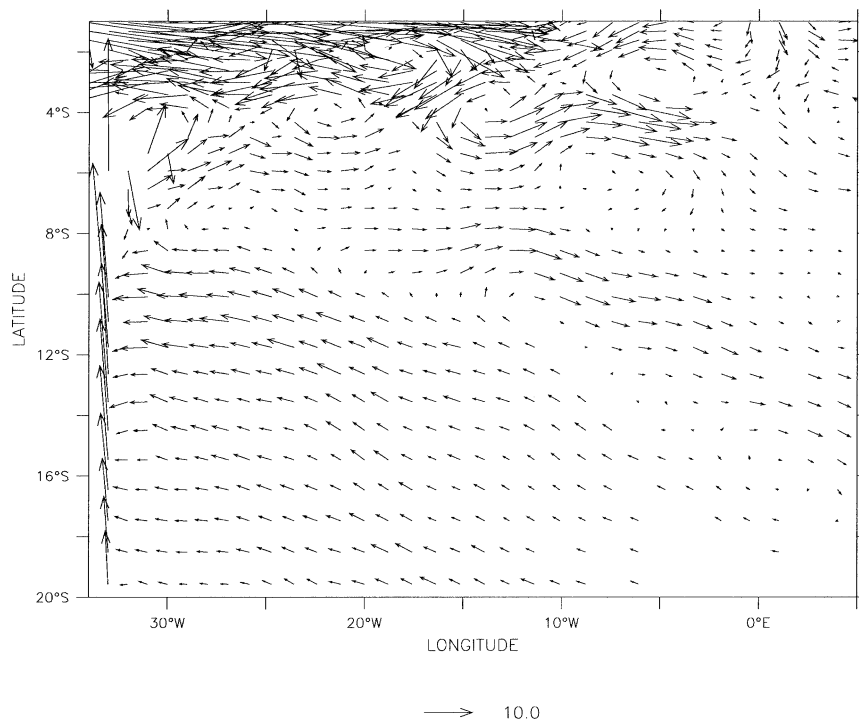


FIG. 9. A Jan snapshot of the velocity (cm s^{-1}) on the 17°C isotherm.

SEUC at 5°S separate at 25°W, much earlier than in the annual mean. At 5°W, this leads to two different cores, similar to those reported in the Pacific by Rowe et al. (2000). In the Atlantic, there are unfortunately no interior ADCP sections beyond 6°S to confirm the existence of this secondary core. The early separation of the cores reinforces the idea that the SEUC may actually have two dynamically different forcing mechanisms. The southeastward flow that constitutes the secondary core closely resembles the results of McCreary et al. (2003); in fact, their SSSC is located farther away from the equator than the observed primary core, just as the present solution suggests. The northern core at 5°S, which is the focus of the present study, appears to be closely connected to the waves between the equator and 5°S. The next section will investigate the source and importance of these eddy fluxes.

4. Wave–zonal flow interaction

In our opinion, the theories that were outlined in the introduction are not sufficient to explain the structure of the SEUC. The observations by Rowe et al. (2000) and the present model results suggest that eddies or waves might be driving at least a part of the SEUC. Here it is shown quantitatively that eddy fluxes maintain the SEUC against dissipation. This section is based on an analysis of the quasigeostrophic (QG) equations. The low Rossby number in the model (0.05) clearly justifies their use to analyze the model results. The observed Rossby number (0.2–0.4) stretches the validity of the QG assumptions, but as demonstrated below, the QG equations are such a powerful tool that they should not be abandoned easily. While this section identifies the driving mechanism for the SEUC in the present model, we concede that in the ocean there might be other processes that are not represented in this model solution.

Waves can have two distinct effects on the mean flow: they accelerate the flow directly through the convergence of eddy momentum flux, and they change the isothermal slope through the flux of heat. It is difficult to estimate the relative contribution of these effects on the mean flow. Only for the case of a zonally averaged flow has it been possible to develop a framework for such a comparison. This framework is called the transformed Eulerian mean (TEM) equations, and it is discussed here to guide our understanding of eddy fluxes. For a more detailed discussion, the reader is referred to the original works by Eliassen and Palm (1961) and Andrews and McIntyre (1976).

The main purpose of zonally averaging the equation of motion around a latitude circle is that the zonal pressure gradient and the mean advection of tracer and momentum vanish (by continuity \bar{v} has to vanish). The zonal derivatives of the eddy fluxes vanish as well. Within the QG framework, the vertical advection of momentum is neglected, yielding the following equation for the zonal momentum:

$$\bar{u}_t - f\bar{v}^a = F - \overline{(v'u')_y}, \quad (1)$$

where u_t is the acceleration of the zonal flow, f is the Coriolis force, v^a is the ageostrophic meridional velocity, F is the friction, and the primes denote the deviation from the zonal mean. The overbars indicate the zonal mean around a latitude circle. The resulting temperature equation is

$$\bar{T}_t + \bar{w}\bar{T}_z = -\overline{(v'T')_y} + H, \quad (2)$$

where T is temperature, w is vertical velocity, and H is the heating. The zonal averaging reduces the continuity equation to

$$\bar{v}_y^a + \bar{w}_z = 0. \quad (3)$$

Equations (1) and (2) show that for the steady state and in the absence of friction and heating, the eddies will induce a meridional overturning circulation. To consider a more general case, w is rewritten as

$$w^* = \bar{w} - \frac{1}{\bar{T}_z} \overline{(v'T')_y}. \quad (4)$$

Since the zonal averaging reduced the continuity equation to two dimensions, it is possible to compute v^* from (3) and w^* :

$$v^* = \bar{v}^a - \left[\frac{1}{\bar{T}_z} \overline{(v'T')_y} \right]_z. \quad (5)$$

Equation (1) can then be rewritten as

$$\bar{u}_t - f v^* = F - \overline{(v'u')_y} + f \left[\frac{1}{\bar{T}_z} \overline{(v'T')_y} \right]_z, \quad (6)$$

where v^* and w^* are commonly referred to as residual mean velocities. The last two terms on the rhs constitute the divergence of the Eliassen–Palm flux and they quantify the acceleration of the zonal flow (u_t) by the eddies. This formulation makes it possible to compare the relative impact of dissipative, thermal and direct momentum forcing on the zonal flow.

The application of this theory to the SEUC in the model is not straightforward because it is not reasonable in the ocean to average around a latitude circle. It is, however, possible to use the ideas of TEM if only a special area of the SEUC is analyzed. It is shown in the previous section that the SEUC, in the model and to a lesser extent in the observations, is in geostrophic balance and is driven by the meridional pressure gradient. Because the geostrophic equations are degenerate, only the next higher order of the equations of motion can explain the origin of the meridional pressure and density gradient: the QG equations (Pedlosky 1987).

The first order balance for the zonal momentum is

$$\bar{u}\bar{u}_x + \bar{v}\bar{u}_y - f\bar{v}^a = F - \overline{(v'u')_y} - \overline{(u'u')_x}. \quad (7)$$

The difference from (1) is that the overbar denotes a *time* average rather than a *zonal* average and that the QG approximations have to be valid to separate between

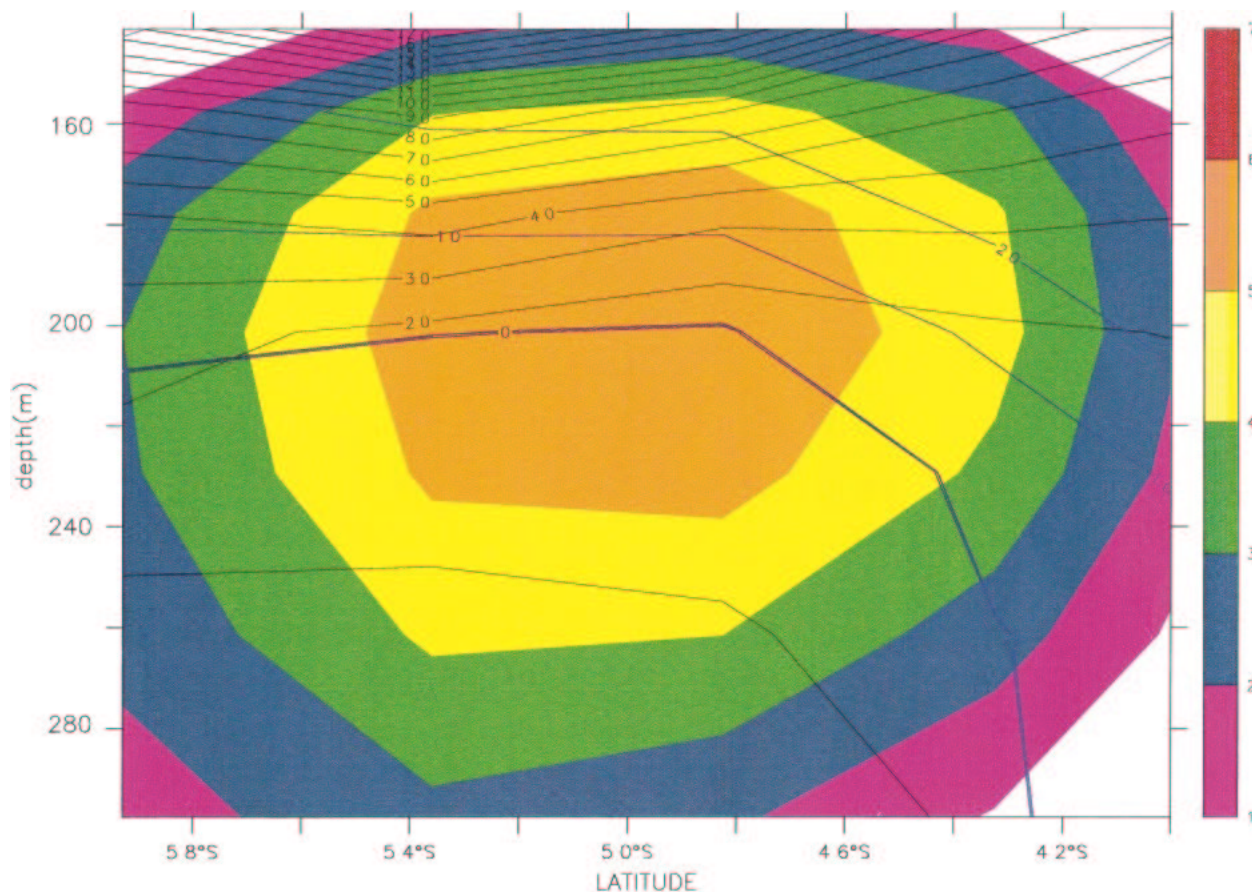


FIG. 10. The zonal velocity in the core of the SEUC at 25°W (cm s^{-1}). Superimposed are the contour lines of the Eliassen–Palm flux convergence (black) and the mean momentum advection (blue; contour lines every 10^{-9} m s^{-2}). The Eliassen–Palm flux convergence is defined strictly only in the core of the SEUC (see later in the text); however, the figure illustrates that in the core of the SEUC the mean advection of momentum is negligible.

the zero- and first-order momentum balance. Crucial to the application of the TEM ideas is the reduction of the continuity equation to two dimensions and the smallness of the nonlinear terms (uu_x, vv_y). It turns out that these conditions are met in the interior along the core of the SEUC, the line of maximum velocity where u_x and u_y are both 0 (Fig. 8). West of 28°W the flow is dominated by the western boundary regime and east of 10°W the flow starts to shift poleward and enters the Ekman layer (Figs. 5 and 8). Between 28° and 10°W, however, the QG approximations hold because the Rossby number is approximately 0.05 and the ratio between the layer depth and its deviation approximately 0.1. In this area, along the core of the SEUC, u_y has to be zero by definition. Because the core of the SEUC shoals toward the east, u_x has to be zero as well (along the core). For example, at the western boundary at 150-m depth the zonal flow is westward but becomes larger (more eastward) farther east (Fig. 8). The zonal flow continues to become larger farther east, vanishes at approximately 27°W and becomes maximal at 15°W, at the core of the SEUC. Further east the zonal flow becomes weaker again. There-

fore, u_x has to be zero right at the core. This important fact, that u_x is 0 at the core, is not a general law; but it happens to be true for the SEUC, because the SEUC shoals on its way to the east. If the core depth would not change, $u_x = 0$ would not be true all along the core but only at one or more points along the core. Figure 10 and Fig. 12 (later in the text) provide a verification for our reasoning from the model results.

After these preparations we can now exploit the special properties of the SEUC core to discuss the connection between the Eliassen–Palm flux and the SEUC. Since along the SEUC core u_x and u_y are 0, (3) remains unchanged apart from replacing the zonal average by a temporal average. Equation (7) reduces to

$$-f\bar{v}^a = F - \overline{(v'u')_y} - \overline{(u'u')_x}. \quad (8)$$

With $\overline{(u'T')_x} \ll \overline{(v'T')_y}$ (Fig. 11), the temperature balance becomes

$$\bar{w}T_z = -\overline{(v'T')_y} - \bar{v}T_y - \bar{u}T_x + H. \quad (9)$$

The vertical velocity can, as in TEM, be rewritten as

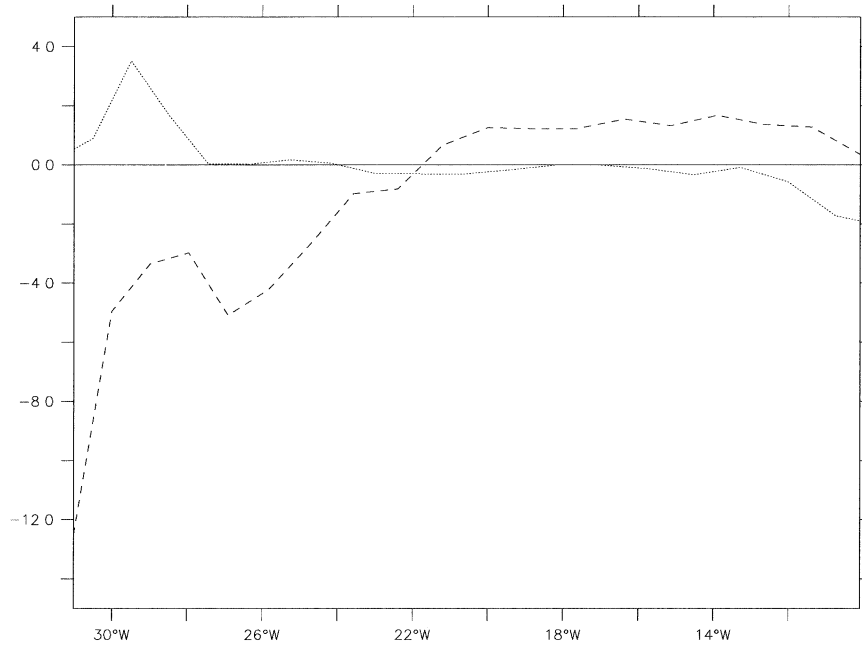


FIG. 11. Strength of meridional (broken line) and zonal (dotted line) eddy temperature flux along the core of the SEUC (10^{-7} K s^{-1}). The meridional flux is dominating over most of the core area.

$$w^* = \bar{w} - \frac{1}{T_z} \overline{(v'T')_y}. \quad (10)$$

The main reason for looking only at the flow along the line of maximum velocity is that it is now possible to use (3) to determine the meridional residual circulation (like in TEM) as

$$v^* = \bar{v}^a - \left[\frac{1}{T_z} \overline{(v'T')} \right]_z. \quad (11)$$

The equation for the zonal momentum [(8)] can now be rewritten as

$$f v^* = k^z u_{zz} + k^y u_{yy} - \overline{(u'u')_x} - \overline{(v'u')_y} + f \left[\frac{1}{T_z} \overline{(v'T')} \right]_z; \quad (12)$$

$k^z u_{zz}$ and $k^y u_{yy}$, the vertical and horizontal dissipation, are the components of F . With this equation it is now possible to determine the relative importance of eddy heat flux, eddy momentum flux, and dissipation in the core of the SEUC: The effect of the eddy heat flux dominates the convergence of eddy momentum flux; the meridional and vertical viscosity are of equal importance (Fig. 12). Between the western boundary regime west of 28°W and the Ekman regime east of 10°W , the eddy fluxes are balanced by friction (Fig. 13), and the residual is supporting a weak meridional circulation v^* of the order of 10^{-4} m s^{-1} .

By computing the geostrophic velocity via the pressure gradient it is in principle possible to arrive at an

independent estimate of the ageostrophic velocity v^a and the residual v^* . However, the rigid-lid formulation of the model does not require and calculate the sea surface height necessary for this calculation. It is possible to recover the surface pressure from the equation of motion, but to do this, the very eddy fluxes that were just evaluated would have to be used. Therefore, without the surface pressure there is no independent way to calculate the ageostrophic velocity.

The analysis of the first-order momentum equation along the core of the SEUC demonstrates that between 28° and 10°W the SEUC is maintained against dissipation by the convergence of the Eliassen–Palm flux. The next section discusses the source of these fluxes.

5. Tropical instability waves

The analysis in the previous section shows that the SEUC is maintained against friction by the eddy heat fluxes which steepen the slope of the isotherms. The remaining problem is to determine the source of these eddy fluxes. The comparison of Exp1 with Exp3 (steady wind) shows that the time mean of the SEUC is the same in both cases (not shown). This suggests that the seasonal Rossby waves are not driving the SEUC. This, and the absence of the SEUC in the linear experiment suggests that the waves which drive the SEUC are generated by instabilities. Therefore the SEUC has to break down after the nonlinear terms in the model are switched off. A decay time can be estimated from a simple scaling argument, with

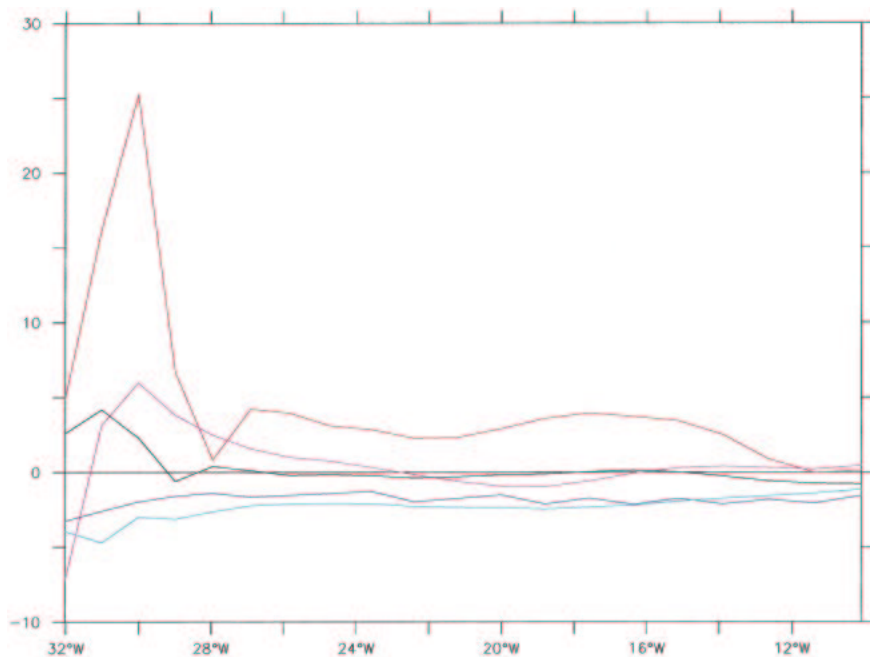


FIG. 12. The contribution of the different terms in (12) to the zonal momentum budget (along the core of the SEUC; 10^{-9} m s^{-2}). The red line shows the contribution of the eddy heat flux, the purple line is the sum of the two eddy momentum flux convergence terms, the dark blue line is the effect of vertical viscosity, and the light blue line shows the effect of meridional viscosity. The black line shows the contribution of mean momentum advection. Theoretically its value should be exactly 0 along the core (see text); its slight deviation from 0 is due to the numerical differencing and the inaccuracies in the algorithm that determines the exact location of the jet core.

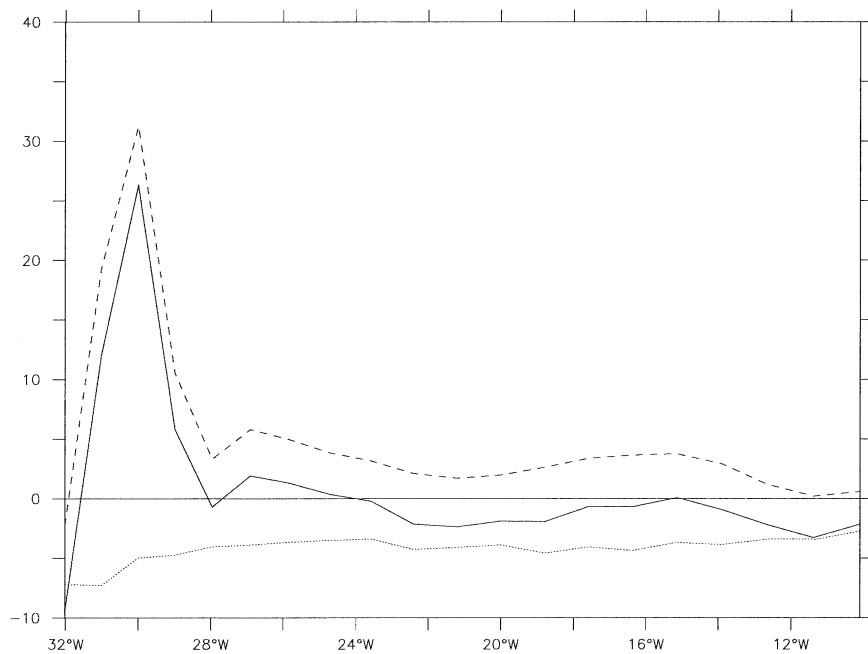


FIG. 13. As in Fig. 11, but for the sum of eddy flux contribution (broken line), the friction (dotted line), and the sum of friction and eddy flux contribution (solid line).

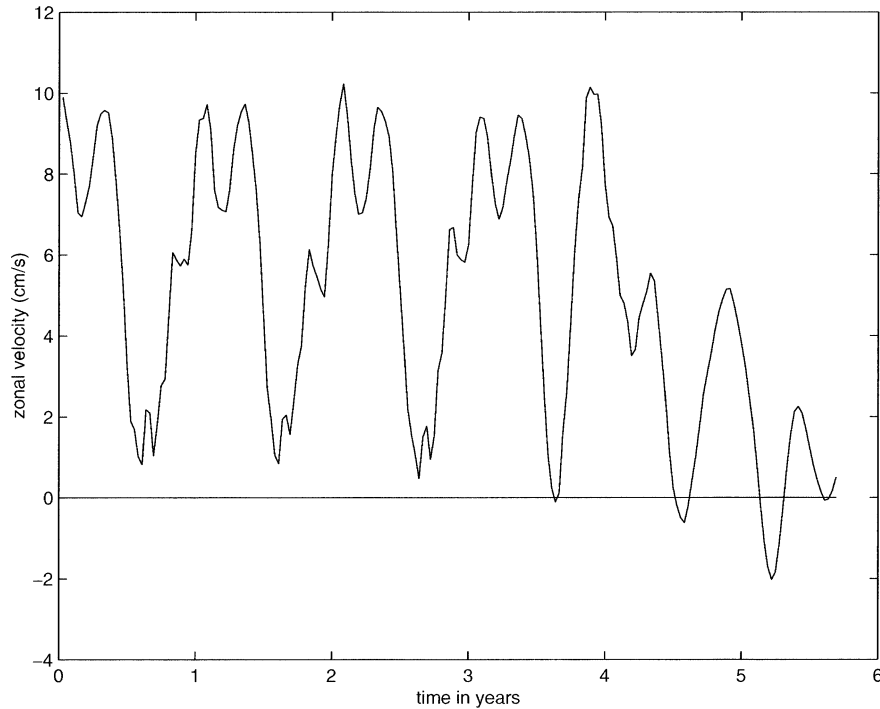


FIG. 14. Low-pass-filtered zonal velocity at 25°W in the core of the SEUC (cm s^{-1}). The nonlinear terms were switched off after year 4. Note that the velocity is the sum of the SEUC mean, the instantaneous zonal flow of the instability waves, and the seasonal Rossby waves.

$$u_i = k^y u_{yy} + k^z u_{zz}, \quad (13)$$

the model's viscosity, and the length scales of the SEUC, the expected decay time is approximately 1 yr. Figure 14 shows the zonal velocity at the core of the SEUC at 25°W , and as predicted by the scale analysis, the SEUC decays within a year after the nonlinear terms are switched off.

The instability theories are based on QG scaling and break down close to the equator, but McCreary and Yu (1992), Yu et al. (1995), Masima and Philander (1999), and Jochum et al. (2003) studied the development of instabilities in the equatorial waveguide with numerical models. They show that instabilities develop along the regions of strong shear between the SEC and EUC. The resulting waves compare well to the observations (e.g., Legeckis 1977) and are commonly referred to as Legeckis waves or TIWs. Figure 15 shows a snapshot of the TIWs in this model. Their zonal wavelength is approximately 1100 km and their period is approximately 1 month, which is close to the observations by Weisberg et al. (1979) who found at 5°W waves with a wavelength of 1220 km and a period of 31 days. Comparison with Weisberg and Weingartner (1988) and Weisberg and Horigan (1981) suggests, however, that the TIWs in the present model are too weak by approximately 20%.

Apart from the results of the linear and the steady-wind experiments, further evidence for the TIWs driving the SEUC can be found in the structure of the TIWs.

The latitude–depth structure of these TIWs can be seen in Fig. 16, which shows the first EOF of the meridional velocity at 25°W ; the corresponding time series is shown in Fig. 17. Figure 16 demonstrates that along the depth range of the SEUC and the NEUC, the latitudes of the SEUC and NEUC cores coincide with the latitudes of the off-equatorial extrema of the TIWs. Moreover, the longitude–depth structure of the TIWs demonstrates that the maxima of the meridional velocity of the TIWs aligns with the core of the SEUC (Fig. 18). This is consistent with a more idealized study by Proehl (1990) who shows that equatorial wave-mean flow interaction creates off-equatorial maxima of Eliassen–Palm flux convergence.

The absence of the SEUC in the linear experiment, the insensitivity of the mean SEUC to the existence of a seasonal cycle, and the particular location of the amplitude maxima of the TIWs leads us to the conclusion that the wave energy that drives the SEUC is provided by the TIWs. Thus, it is the particular structure of the TIWs that leads to maxima in the convergence of the Eliassen–Palm flux at approximately 5°S and 4°N , thereby determining the position of the SEUC. The diapycnal structure of the core of the SEUC can then be explained by the westward and downward propagation of the TIWs; water does not move across isopycnals along the core of the SEUC from west to east—instead it is locally provided by the TIWs and has a strong oscillatory meridional velocity component.

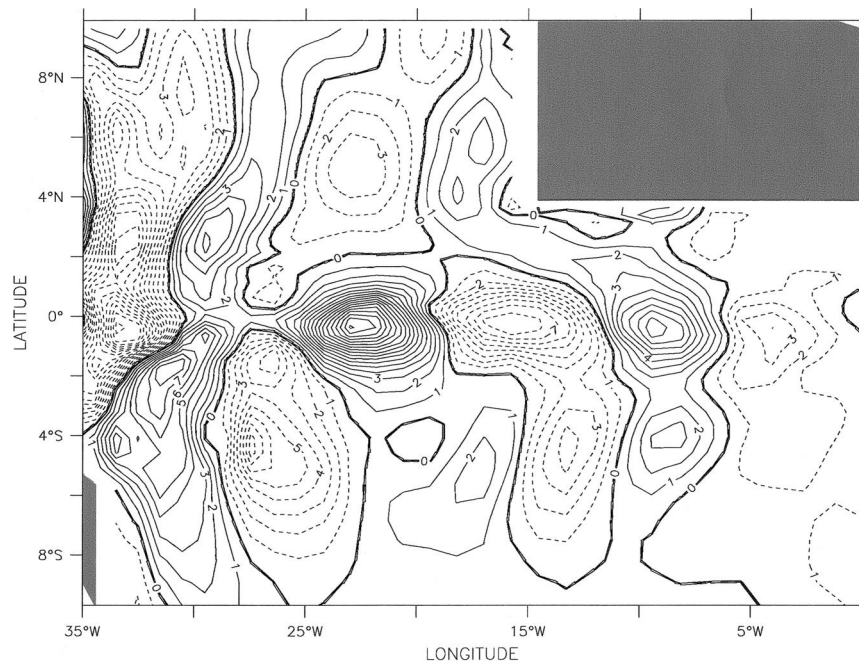


FIG. 15. A snapshot of meridional velocity anomalies on the 17°C isotherm (cm s^{-1}).

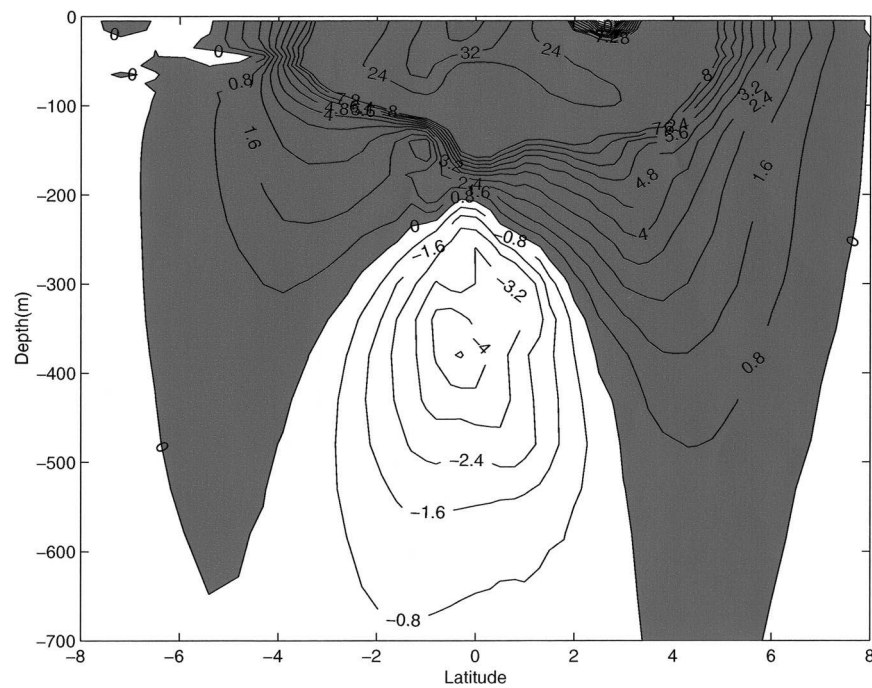


FIG. 16. The first EOF of the meridional velocity (cm s^{-1}) at 25°W. This mode explains 56% of the variability (the second mode explains 17%). The shaded area indicates positive values, and the white area shows negative values. Note how below 150-m depth the off-equatorial extrema of the EOF coincide with the latitudes of the SEUC and NEUC. The SEUC core at this longitude has a depth of 200 m. The position of the subthermocline extrema does not change with longitude.

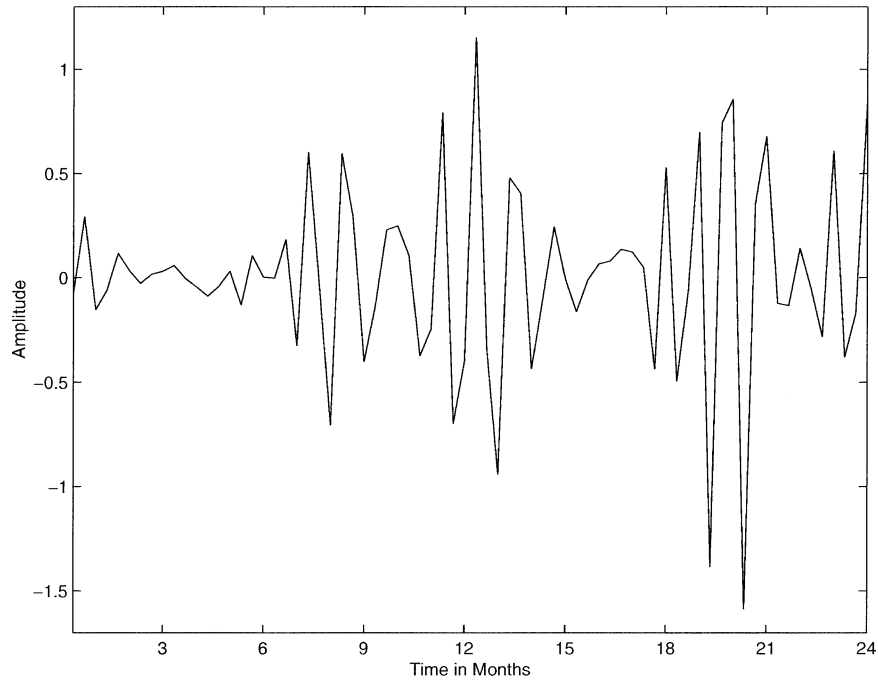


FIG. 17. A 2-yr section of the time series that corresponds to the EOF in Fig. 15.

At first sight this connection between the TIWs and the SEUC is counterintuitive, because the TIWs are thought be generated slightly north of the equator in the eastern part of the basin (Chelton et al. 2000). However, we find in our study that the instabilities that are excited

in the mixed layer project on equatorially symmetric Rossby and Yanai waves, which radiate energy eastward and westward away from the source of the instabilities. This is in agreement with findings by Masina et al. (1999) for the Pacific Ocean.

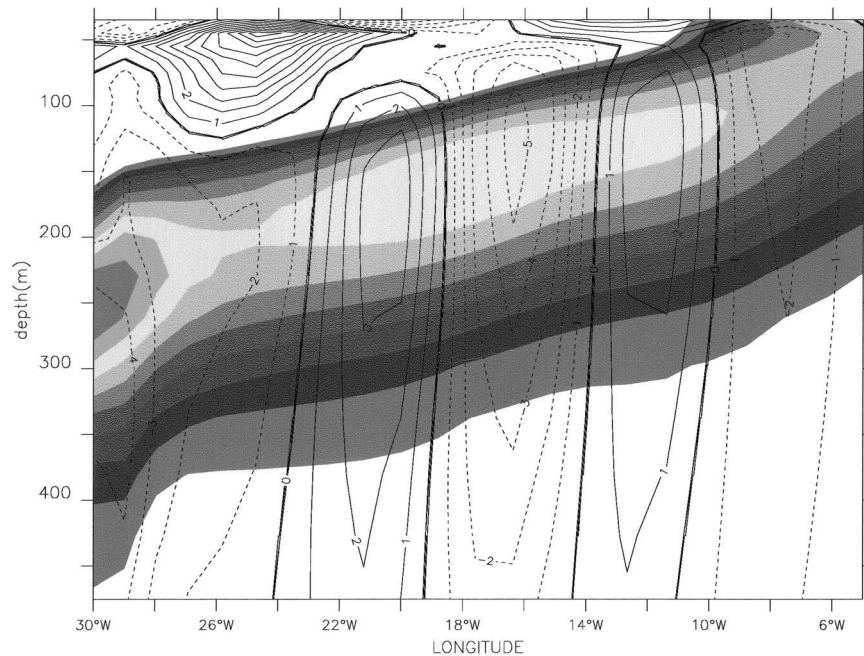


FIG. 18. Snapshot of the meridional velocity anomaly (cm s^{-1}) of the TIWs at 5°S superimposed on the core of the SEUC. Note how the velocity maxima align with the depth of the core. Shading interval is 1 cm s^{-1} .

6. Summary and discussion

A numerical simulation of the tropical Atlantic Ocean is used to investigate the relevance of eddy fluxes for the SEUC. The study focuses on the SEUC dynamics away from the NBC recirculations (east of 28°W) and west of 10°W where the SEUC core enters the Ekman and the mixed layer. In this area the SEUC in the model (and to a lesser degree in the observations) is in geostrophic balance and the flow is to the lowest order along isopycnals. On the lighter isopycnals, the flow is not connected to the western boundary (Fig. 8); therefore some of the SEUC water has to be provided by another source—the EUC (Fig. 6).

The flow in the present study looks similar to the results of McCreary et al. (2003), which explains the SEUC as the result of arrested Rossby wave fronts. However, the present study suggests that in addition to the McCreary et al. (2003) mechanism, there is a second mechanism that can drive the SEUC: the Eliassen–Palm flux of the TIWs. Three pieces of evidence for this theory are presented. First, after removal of the advection of momentum in the model equations, the TIWs as well as the well-defined core of the SEUC vanish. Second, a quantitative analysis of the zonal momentum equation along the core of the SEUC shows that the SEUC is maintained against dissipation by the convergence of the wave-induced Eliassen–Palm flux. Last, the position of the off-equatorial extrema of the TIWs coincides with the location of the SEUC. Our understanding of the present results is that the meridional heat flux that is associated with the TIWs steepens the isopycnals and thereby generates a geostrophically balanced flow, which is limited by dissipation. We furthermore suspect that this interplay between dissipation and eddy fluxes is the physical process behind the secondary circulation introduced ad hoc by Marin et al. (2000). However, a detailed comparison between their assumptions and our model results is beyond the scope of this study.

An obvious limitation of the present study is that the modeled SEUC is only one-half as strong as the observed SEUC. The authors are not aware of any model study that represents the Atlantic or the Pacific SSC adequately. However, this very fact and the present result offer a simple explanation. The SEUC strength depends on TIW strength and viscosity. Furthermore, the TIWs have to have the right structure to generate the Eliassen–Palm flux convergence in the right location. Since the meridional viscosity in eddy-resolving models has no physical but only a numerical justification, the dissipation in the model is certainly too high, which would make the TIWs in the model too weak and the SSCs even more so. Friction in the ocean has been and still is very difficult to observe, which makes this part of our theory difficult to verify or disprove. Therefore, our future research will focus on the structure of the TIWs. Linear planetary waves do not generate a net meridional heat flux, the TIWs do. How can we explain

the particular structure of the TIWs and how sensitive is it to external forcing?

In the present work we focused for obvious reasons on the SEUC. The similar structure of NEUC and the SCCs suggests that the Eliassen–Palm flux of the TIW is important for them as well. This conjecture, however, demands verification.

Acknowledgments. We are grateful to Raffaele Ferrari for many insightful discussions; furthermore, we benefited from the helpful suggestions of Tony Busalacchi, Glenn Flierl, Breck Owens, and Mike Spall. Comments from Jay McCreary, Greg Johnson, Mike McPhaden, and one anonymous reviewer helped to improve the manuscript considerably. The computations have been performed at the NCAR facilities in Colorado, and this research was funded with NOAA Grant NA16GP1576 and NASA Grant NAG5-7194 at MIT.

REFERENCES

- Andrews, D. G., and M. E. McIntyre, 1976: Planetary waves in horizontal and vertical shear: The generalized Eliassen–Palm relation and the mean zonal acceleration. *J. Atmos. Sci.*, **33**, 2031–2048.
- Bourles, B., M. D’Orgeville, G. Eldin, Y. Gouriou, R. Chuchla, Y. DuPenhoat, and S. Arnault, 2002: On the evolution of the thermocline and subthermocline eastward currents in the equatorial Atlantic. *Geophys. Res. Lett.*, **29**, 1785, doi:10.1029/2002GLO15098.
- Chelton, D. B., F. J. Wentz, C. L. Gentemann, R. A. de Szoeke, and M. G. Schlax, 2000: Satellite microwave SST observations of transequatorial tropical instability waves. *Geophys. Res. Lett.*, **27**, 1239–1242.
- Cochrane, J. D., F. J. Kelly, and C. R. Olling, 1979: Subthermocline countercurrents in the western equatorial Atlantic Ocean. *J. Phys. Oceanogr.*, **9**, 724–738.
- Donohue, K. A., E. Firing, G. D. Rowe, A. Ishida, and H. Mitsudera, 2002: Equatorial Pacific subsurface countercurrents: A model–data comparison in stream coordinates. *J. Phys. Oceanogr.*, **32**, 1252–1264.
- Eliassen, A., and E. Palm, 1961: On the transfer of energy in stationary mountain waves. *Geofys. Publ.*, **22**, 1–23.
- Hansen, D. V., and C. A. Paul, 1984: Genesis and effects of long waves in the equatorial Pacific. *J. Geophys. Res.*, **89**, 10 431–10 440.
- Hellerman, S., and M. Rosenstein, 1983: Normal monthly wind stress over the World Ocean with error estimates. *J. Phys. Oceanogr.*, **13**, 1093–1104.
- Hua, B. L., F. Marin, and R. Schopp, 2003: Three-dimensional dynamics of the subsurface countercurrents and equatorial thermocline. Part I: Formulation of the problem and generic properties. *J. Phys. Oceanogr.*, **33**, 2588–2609.
- Jochum, M., 2002: On the pathways of the return flow of the meridional overturning circulation in the tropical Atlantic. Ph.D. thesis, Massachusetts Institute of Technology, 139 pp.
- , and P. Malanotte-Rizzoli, 2001: Influence of the meridional overturning circulation on the tropical–subtropical pathways. *J. Phys. Oceanogr.*, **31**, 1313–1323.
- , and —, 2003: On the generation of North Brazil current rings. *J. Mar. Res.*, **61**, 147–162.
- , —, and A. Busalacchi, 2003: Tropical instability waves in the Atlantic Ocean. *Ocean Modell.*, in press.
- Johnson, G. C., and D. W. Moore, 1997: The Pacific subsurface countercurrents and an inertial model. *J. Phys. Oceanogr.*, **27**, 2448–2459.

- Kroeger, J., 2001: Mechanismen meridionaler transportprozesse im tropischen Atlantik. Ph.D. dissertation, IFM Kiel, 153 pp.
- Legeckis, R., 1977: Long waves in the eastern equatorial Pacific Ocean: A view from a geostationary satellite. *Science*, **197**, 1179–1181.
- Liu, Z., and S. G. H. Philander, 1995: How different wind stress patterns affect the tropical–subtropical circulations of the upper ocean. *J. Phys. Oceanogr.*, **25**, 449–462.
- Marin, F., B. L. Hua, and S. Wacogne, 2000: The equatorial thermostat and subsurface countercurrents in the light of atmospheric Hadley cell dynamics. *J. Mar. Res.*, **58**, 405–437.
- , R. Schopp, and B. L. Hua, 2003: Three-dimensional dynamics of the subsurface countercurrents and equatorial thermostat. Part II: Influence of the large-scale ventilation and of equatorial winds. *J. Phys. Oceanogr.*, **33**, 2610–2626.
- Masina, S., and S. G. H. Philander, 1999: An analysis of tropical instability waves in a numerical model of the Pacific Ocean, 1, Spatial variability of the waves. *J. Geophys. Res.*, **104**, 29 613–29 635.
- , —, and A. B. G. Bush, 1999: An analysis of tropical instability waves in a numerical model of the Pacific Ocean, 2, Generation and energetics of the waves. *J. Geophys. Res.*, **104**, 29 613–29 635.
- Mayer, D. A., R. L. Molinari, and J. F. Festa, 1998: The mean and annual cycle of upper layer temperature fields in relation to Sverdrup dynamics within the gyres of the Atlantic Ocean. *J. Geophys. Res.*, **103**, 18 545–18 566.
- McCreary, J. P., 1981: A linear stratified ocean model of the equatorial undercurrent. *Philos. Trans. Roy. Soc. London*, **298**, 603–645.
- , and Z. Yu, 1992: Equatorial dynamics in a 2.5-layer model. *Progress in Oceanography*, Vol. 29, Pergamon, 61–132.
- , P. Lu, and Z. Yu, 2002: Dynamics of the Pacific subsurface countercurrents. *J. Phys. Oceanogr.*, **32**, 2379–2404.
- McPhaden, M. J., 1984: On the dynamics of equatorial subsurface countercurrents. *J. Phys. Oceanogr.*, **14**, 1216–1225.
- Oliger, O., and A. Sundstrom, 1978: Theoretical and practical aspects of some initial boundary value problems in fluid dynamics. *J. Appl. Math.*, **35**, 419–446.
- Pedlosky, J., 1987: *Geophysical Fluid Dynamics*. Springer-Verlag, 710 pp.
- Philander, S. G., 1990: *El Niño, La Niña and the Southern Oscillation*. Academic Press, 293 pp.
- Proehl, J. A., 1990: Equatorial wave–mean flow interaction: The long Rossby waves. *J. Phys. Oceanogr.*, **20**, 274–294.
- Rowe, P. B., E. Firing, and G. C. Johnson, 2000: Pacific equatorial subsurface countercurrent velocity, transport and vorticity. *J. Phys. Oceanogr.*, **30**, 1172–1187.
- Schmitz, W. J., and M. S. McCartney, 1993: On the North Atlantic circulation. *Rev. Geophys.*, **31**, 29–49.
- Schott, F. A., L. Stramma, and J. Fischer, 1998: Transports and pathways of the upper-layer circulation in the western tropical Atlantic. *J. Phys. Oceanogr.*, **28**, 1904–1928.
- Spall, M. A., and A. R. Robinson, 1989: A new open ocean, hybrid coordinate primitive equation model. *Math. Comput. Simul.*, **31**, 241–269.
- Stevens, D. P., 1990: On open boundary conditions for three dimensional primitive equation ocean circulation models. *Geophys. Astrophys. Fluid Dyn.*, **51**, 103–133.
- Stroup, E. D., 1954: Mid-Pacific oceanography, Part IV. *U.S. Fish Wildl. Ser. Spec. Sci. Rep.*, **135**, 17–31.
- Tsuchiya, M., 1975: Subsurface countercurrents in the eastern equatorial Pacific Ocean. *J. Mar. Res.*, **33** (Suppl.), 145–175.
- Weisberg, R. H., and A. M. Horigan, 1981: Low-frequency variability in the equatorial Atlantic. *J. Phys. Oceanogr.*, **11**, 913–920.
- , and T. J. Weingartner, 1988: Instability waves in the equatorial Atlantic Ocean. *J. Phys. Oceanogr.*, **18**, 1641–1657.
- , A. Horigan, and C. Colin, 1979: Equatorially trapped Rossby-gravity wave propagation in the Gulf of Guinea. *J. Mar. Res.*, **37**, 67–86.
- Yu, Z., J. P. McCreary, and J. Proehl, 1995: Meridional asymmetry and energetics of tropical instability waves. *J. Phys. Oceanogr.*, **25**, 2997–3007.